TREASURES @UT Dallas

UT DALLAS | Eugene McDermott Library

Erik Jonsson School of Engineering and Computer Science

2014-08

Effective Sensing of RDX via Instant and Selective Detection of Ketone Vapors

UTD AUTHOR(S): Kui Tan and Yves J. Chabal

©2014 The Royal Society of Chemistry. This article may not be further made available or distributed.

Hu, Zhichao, Kui Tan, William P. Lustig, Hao Wang, et al. 2014. "Effective sensing of RDX via instant and selective detection of ketone vapors." Chemical Science 5(12): 4873-4877.

Find more research and scholarship conducted by the Erik Jonsson School of Engineering and Computer Science here. This document has been made available for free and open access by the Eugene McDermott Library. Contact libwebhelp@utdallas.edu for further information.

Chemical Science

EDGE ARTICLE

View Article Online
View Journal | View Issue

Cite this: *Chem. Sci.*, 2014, **5**, 4873

Effective sensing of RDX *via* instant and selective detection of ketone vapors†

Zhichao Hu,[a] Kui Tan,[b] William P. Lustig,[a] Hao Wang,[a] Yonggang Zhao,[a] Chong Zheng,[c] Debasis Banerjee,[a] Thomas J. Emge,[a] Yves J. Chabal[b] and Jing Li*[a]

Received 19th July 2014
Accepted 16th August 2014

DOI: 10.1039/c4sc02157f

www.rsc.org/chemicalscience

Two new luminescent metal–organic frameworks (LMOFs) were synthesized and examined for use as sensory materials. Very fast and effective sensing of RDX was achieved by vapor detection of a cyclic ketone used as a solvent in the production of plastic explosives. The effects of porosity and electronic structure of the LMOFs on their sensing performance were evaluated. We demonstrate that the optimization of these two factors of an LMOF can significantly improve its sensitivity and selectivity. We also elucidate the importance of both electron and energy transfer processes on the fluorescence response of a sensory material.

Introduction

The detection of energetic materials has attracted much attention over the past decade.[1–4] RDX (1,3,5-trinitroperhydro-1,3,5-triazine) a common explosive in terrorist activities, is of great current interest due to the enormous difficulty in its detection.[5] First, the vapor pressure of RDX is extremely low (6 ppt or 4.6×10^{-9} Torr).[6,7] This issue is compounded by the presence of binders and other components, which reduces the weight percent of the explosive molecule and further decreases the vapor pressure. Furthermore, it is estimated that the vapor pressure of the explosive molecule can be reduced by a factor of 1000 in the presence of wrapping or packing materials.[6] Finally, the unfavorable reduction potential and the absence of an aromatic ring in RDX further diminish its capability to interact with a sensory material, making its effective detection extremely challenging.[3,8,9] A feasible alternative to identifying the explosives is to detect volatile species in their headspace, such as plasticizers, stabilizers, solvents, and degradation products, which may make easier targets.[9–12]

Luminescent metal–organic frameworks (LMOFs) made their debut as explosives sensors very recently.[13–15] In comparison to conjugate polymers, LMOFs are unique in the following aspects: high crystallinity, intrinsic porosity, and systematically tunable pore surface.[16–23] Engineering these factors can significantly enhance the selectivity and sensitivity of a LMOF material towards a specific target. The first study on explosive detection utilizing a LMOF material, LMOF-111 (or RPM3-Zn, $Zn_2(bpdc)_2(bpee)$, bpdc = 4,4′-biphenyldicarboxylate, bpee = 1,2-bis(4-pyridyl)ethylene), showed that it is capable of very fast, sensitive, and reversible detection of DMNB (2,3-dimethyldinitrobutane) and DNT (2,4-dinitrotoluene) in the vapor phase.[13,14] Following this work, a more systematic investigation on LMOF-121 ($Zn_2(oba)_2(bpy)$, oba = 4,4′-oxybis(benzolate), bpy = 4,4′-bipyridine) uncovered the excited state electron transfer mechanism for LMOF based sensors.[15] More recently this subject has been expanded to a number of different LMOFs, for the detection of small molecules[24,25] and ionic species,[26–28] as well as explosive species.[29–38] In the cases of explosive sensing, the detection has always been directly of the explosives and/or explosive-like molecules. Herein, we strategically target a solvent (cyclohexanone) that is used in the recrystallization of RDX and inevitably co-exists in the explosive product, as a way of indirect yet faster and easier detection.

Results and discussion

LMOF-201 ($Zn_2(ofdc)_2(bpy)\cdot 2.5DMF\cdot 1.25H_2O$, ofdc = 9-oxo-9*H*-fluorene-2,7-dicarboxylic acid, DMF = *N*,*N*′-dimethylformamide) and LMOF-202 ($Zn_2(hfdc)_2(bpy)\cdot x$DMA, hfdc = 9*H*-fluorene-2,7-dicarboxylic acid, DMA = *N*,*N*′-dimethylacetamide) were synthesized using solvothermal method (SI 1). Single crystal X-ray diffraction revealed that both structures are three-dimensional (3D) frameworks built on $Zn_2(Rfdc)_4$ (R = O or H) paddle-wheel secondary building unit (SBU), as shown in Fig. 1.[39,40] Each SBU is connected to four identical units to form a two-dimensional (2D) 4^4 net. The adjacent 2D layers are further bridged by bpy ligands giving rise to a 6 coordinated

[a]*Department of Chemistry and Chemical Biology, Rutgers University, 610 Taylor Rd., Piscataway, NJ 08854, USA. E-mail: jingli@rutgers.edu; Fax: +1-732-445-5312*

[b]*Department of Material Science and Engineering, University of Texas-Dallas, Richardson, TX 75080, USA*

[c]*Department of Chemistry and Biochemistry, Northern Illinois University, DeKalb, IL 60115, USA*

† Electronic supplementary information (ESI) available: Synthesis, PXRD, TG and gas adsorption data, UV, PL and IR spectra, molecular orbital and band structure calculations *etc.* CCDC 979464 and 979465. For ESI and crystallographic data in CIF or other electronic format see DOI: 10.1039/c4sc02157f

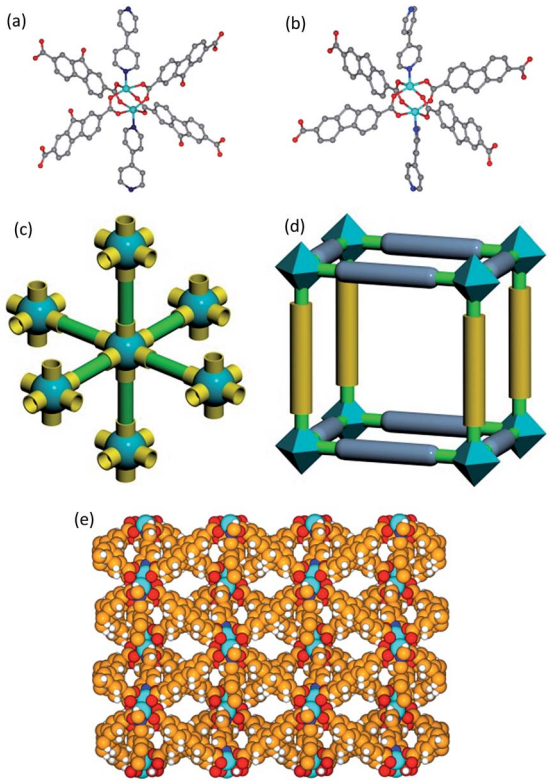

Fig. 1 SBUs of (a) LMOF-201 and (b) LMOF-202; Illustrations of (c) the connectivity of ligands (green) to the Zn core (aqua) and (d) a single cage of the framework; (e) The overall 3D structure of LMOF-202, viewed along the a axis. Colour code: white (H), orange (C), blue (N), red (O), aqua (Zn).

uninodal net with the Point symbol of $\{4^{12}\cdot 6^3\}$ and Vertex symbol of $[4.4.4.4.4.4.4.4.4.4.4.6_4.6_4.6_4]$. Two such 3D networks interpenetrate to yield the overall structure. The compounds can be activated at 120 °C under vacuum overnight (LMOF-201′ and LMOF-202′). Although constructed from similar ligands, the two compounds differ drastically in porosity: While both compounds experience certain degree of structure change upon activation, LMOF-201′ is nearly nonporous in comparison to LMOF-202′ as a result of a larger substitution group on the carboxylate. The BET surface areas are 24 $m^2\ g^{-1}$ and 136 $m^2\ g^{-1}$, respectively.

The photoluminescence (PL) response towards ketone vapors was evaluated on activated solid samples. Both compounds display band-gap emission in the blue/green region primarily due to ligand-to-ligand charge transfer (LLCT). Density of states (DOS) calculations on LMOF-202 revealed that the maximum of valance band (VB) consists mostly of bpy states while the minimum of conduction band (CB) is largely made of the hfdc orbitals (Fig. S22†). A series of chain and cyclic ketones were included in this study. Ketones have high-lying lowest unoccupied molecular orbitals (LUMOs) which are far above the conduction bands of LMOFs (Fig. 4, Tables S6, S8 and S9†). Upon excitation, they act as strong electron donors and therefore enhance the fluorescent emission of LMOFs.[15] The experimental observation of the interaction between LMOF-202′ and the saturated vapor of ketones supports this prediction: the fluorescence intensity of LMOF-202′ was enhanced significantly after only 10 seconds of exposure (with the exception of acetone, Fig. 2). Note that upon exposure to ketone vapors, the emission maximum of LMOF-202′ shifted to higher energy, a strong evidence of exciplex formation.[17] Taking emission peak wavelength and intensity changes into account, each ketone can be pin-pointed on a 2D map as shown in Fig. 3. To further testify that detecting cyclohexanone is a feasible method to indirectly identify RDX, LMOF-202′ was exposed to a sample of RDX recrystallized in cyclohexanone and its PL signals were monitored over a period of time. A considerable enhancement in its emission intensity was observed (more than 12% within 15 minutes). A control experiment on excessively dried RDX (in vacuum oven for 72 hours) gave no PL response (Fig. S16 and S17†). Therefore the residue cyclohexanone is a proven easier target than RDX itself. Besides being able to rapidly identify ketones, another merit of LMOF-202′ is its resistance to

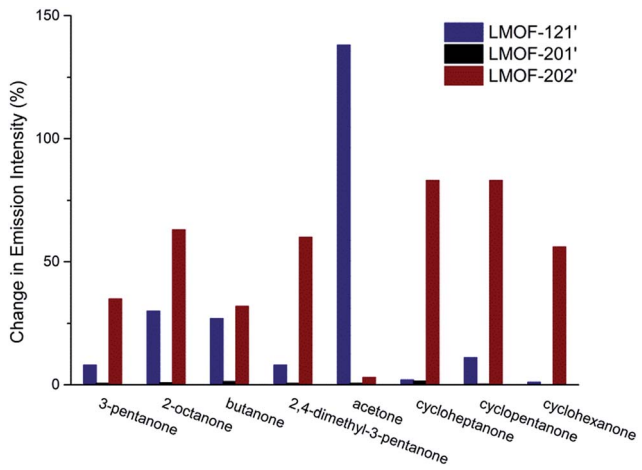

Fig. 2 A comparison of fluorescence enhancement after 10 s exposure of LMOF-121′ and LMOF-202′ to the vapors of ketones.

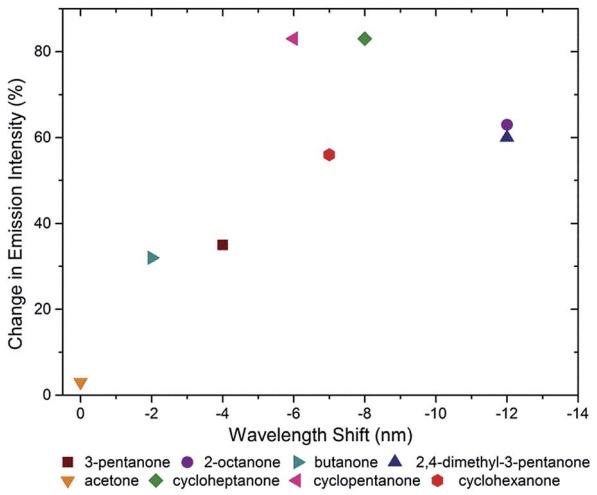

Fig. 3 A 2D colour coded map of ketones based on the fluorescence response of LMOF-202′.

This journal is © The Royal Society of Chemistry 2014

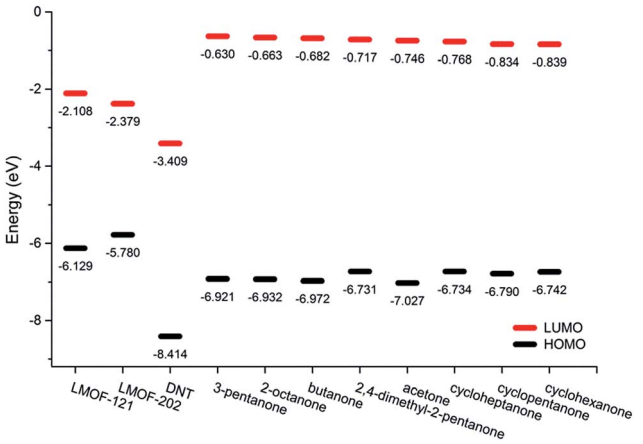

Fig. 4 An illustration of molecular orbital energy levels of LMOF-121, LMOF-202, and analytes computed at B3LYP/SDD (on Zn), 6-31+G*(on H, C, N, O).[41]

interferences from other molecules; common solvents and representative aromatics barely affect its emission (Fig. S18†).

In situ infrared spectroscopy indicates that ketone vapors are captured by LMOF-202′, with the appearance of several new features specifically associated with ketones such as the ν(C═O), $\nu_{as,s}(CH_2)$ and ν(C–C) bands. These bands are red shifted from their positions in the free ketones by ~20 to ~30 cm^{-1} upon adsorption into LMOFs (Fig. 5 and S24†). The adsorption of larger ketone molecules such as 2-octanone, cyclopentanone, and cyclohexanone significantly perturbs the skeleton vibrational modes of LMOF-202′, as seen in red shifts of the stretching modes of the carboxylate group $\nu_{as,s}(COO^-)$ and of the phenyl ring ν_{phenyl}, as shown in Fig. 5 (for reference, the IR spectra of original LMOFs are shown in Fig. S23†). In contrast, the perturbations induced by the inclusion of acetone into LMOF-202′ are much weaker, suggesting a weaker

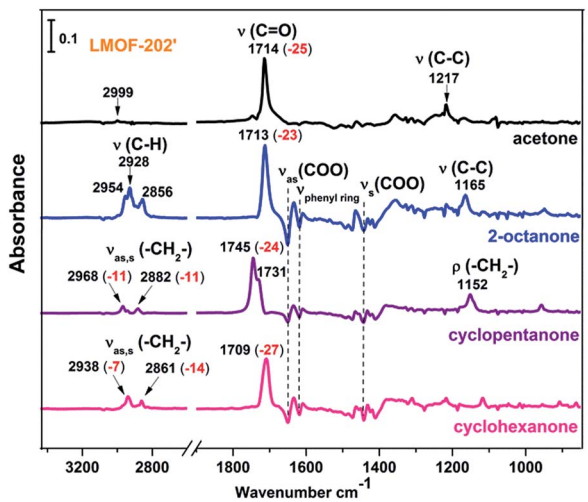

Fig. 5 IR absorption spectra of adsorbed ketone molecules: acetone, 2-octanone, cyclopentanone, cylcohexanone in LMOF-202′ referenced to IR spectrum of blank LMOF-202′. The spectra were recorded after exposing LMOF samples to vapors for 3 min.

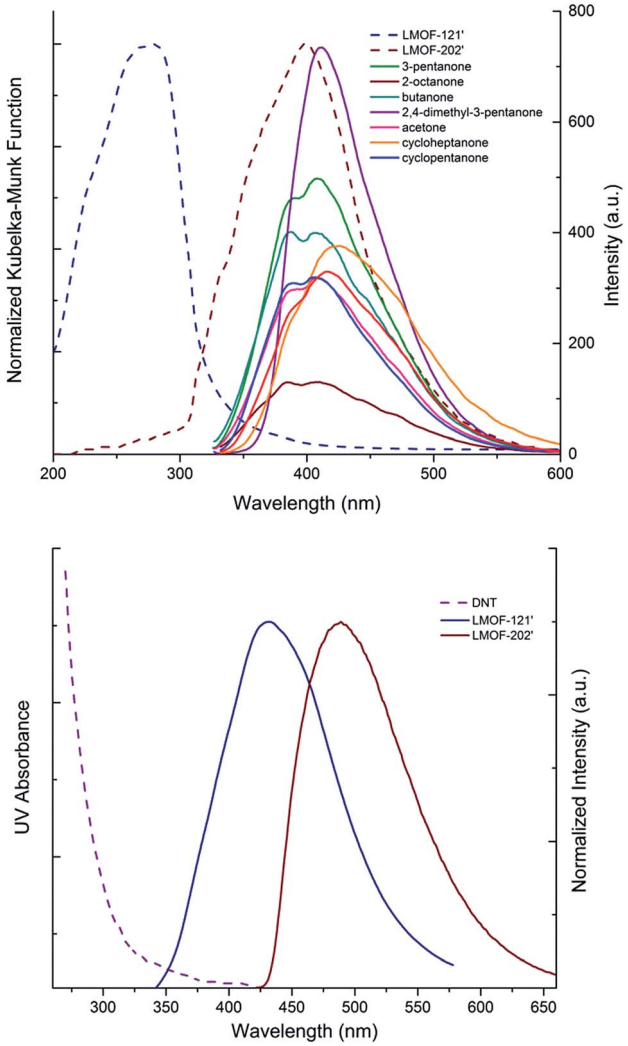

Fig. 6 Top: emission spectra of ketones (solid lines) at λ_{ex} = 300 nm and UV absorbance of LMOF-121′ (dashed blue) and LMOF-202′ (dashed burgundy). Bottom: UV absorbance of DNT (dashed blue) and emission spectra of LMOF-121′ (solid blue, λ_{ex} = 280 nm) and LMOF-202′ (solid burgundy, λ_{ex} = 300 nm).

interaction with this framework. This is consistent with the observation that acetone diffuses out of LMOF-202′ much faster than other longer chain and cyclic ketones (S8, Fig. S26 and S27†). Therefore, the notably low response in fluorescence intensity of LMOF-202′ to acetone vapor is attributed to the weaker interaction (*i.e.* affinity) of this small sized molecule with the framework.

Although LMOF-201′ and LMOF-202′ have very similar band gaps (Fig. S10†), their responses to ketone vapors are distinctly different. LMOF-201′ is quite inert to ketones, as its fluorescence intensity was barely affected upon exposure to ketone vapors. In this case, porosity differentiates the two; the intrinsic pores within the LMOF-202′ facilitate the diffusion and accumulation of analytes, and the confined analytes interact more readily with the sensory material, resulting in enhanced response. This does not apply to LMOF-201′ as it is nearly nonporous.

The role of electron transfer (short-range) process in the change of fluorescence of a LMOF under excitation has been well examined in numerous studies concerning chemical sensing and explosive detection. Yet energy transfer, a long range process vital to the mediation of the fluorescence response, has scarcely been explored. In the case of LMOF-202′ large spectral overlaps were found between its absorption spectrum and the emission spectra of ketones (Fig. 6). A large portion of emitted photons from ketones are re-adsorbed by LMOF-202′ which contributes significantly to the enhancement of its emission. To address the impact of energy transfer, LMOF-121 was selected for comparison. The porosity (surface area) of LMOF-121′ is similar to that of LMOF-202′,but the absorption spectra of the two are very different: LMOF-121′ has a notably higher band gap (~4.0 eV, Fig. S10†) and absorbs in a higher energy region (Fig. 6) than LMOF-202′ (band gap: ~2.5 eV). With the same exposure time (10 seconds), the fluorescence enhancement of LMOF-121′ is generally much less than that of LMOF-202′ (Fig. 2, with a clear exception of acetone). This observation can be partially attributed to the very small spectral overlap between the absorption spectrum of LMOF-121′ and the emission spectra of ketones, limiting the emission enhancement due to the energy transfer effect. On the other hand, large spectral overlaps are attained between the absorption spectrum of LMOF-202′ and the emission spectra of ketones, contributing substantially to the enhancement of PL emission. The exception in the case of acetone may be explained by both IR and adsorption studies. The high compatibility between the pore size of LMOF-121′ and the molecular size of acetone leads to a particularly strong guest–host interaction, and consequently acetone molecules are adsorbed and held much more strongly in LMOF-121′ than in LMOF-202′ (Fig. S26†). This is confirmed by the heat of adsorption (Q_{st}) values calculated from acetone adsorption isotherms, which are ~70–80 kJ mol^{-1} for LMOF-121′ and only ~50–51 kJ mol^{-1} for LMOF-202′ (Fig. S9†). The adsorption/interaction of larger ketones in LMOF-121′ is much limited compared to LMOF-202′ due to its small pore size (Fig. S25 and Table S10†), and thereby much lower PL responses (Fig. 2).

The energy transfer mechanism is more recognized in fluorescence quenching where the emission spectrum of sensory material overlaps with the absorption spectrum of analyte.[33,42,43] To compare the effect of energy transfer on the fluorescence quenching response of LMOF-202 and LMOF-121, fluorescence titrations of DNT (2,4-dinitrotulene) were performed on 0.4 mg mL^{-1} suspensions of LMOF in DMF respectively (Fig. S19 and S20†). The Stern–Volmer (SV) equation, $I_0/I = K_{sv}[Q] + 1$, was employed to evaluate the quenching efficiency of two LMOFs, where I_0 is the initial fluorescence intensity without the quencher, I is the fluorescence intensity with the addition of the quencher, $[Q]$ is the molar concentration of the quencher, and K_{sv} is the quenching constant. For LMOF-121 a K_{sv} of 1.1×10^4 M^{-1} was obtained, which is comparable to the best performance of reported polymer sensors.[44] Using LMOF-121, the detection limited for DNT is estimated to be 4.98 μM or 0.91 μg mL^{-1} (Fig. S19†). For LMOF-202, a smaller K_{sv} value is obtained, 4.6×10^3 M^{-1} (Fig. S20†). This difference is due to both electron and energy transfer effects: Electronically, LMOF-121 has a higher CB than that of LMOF-202, thus favoring electron transfer to DNT at excited state (Fig. 4). Considering energy transfer, LMOF-121 is more sensitive towards DNT because its emission spectrum overlaps much more strongly with the absorption spectrum of DNT than that of LMOF-202. Such spectral overlap is essentially nonexistent for the latter (Fig. 6) and the quenching effect relies solely on electron transfer.

Conclusions

In summary, two new and closely related members of the LMOF family, LMOF-201 and LMOF-202, were synthesized and structurally characterized. Engineering one of the ligand with different functional groups has led to distinctly different porosity between the two compounds, which drastically affects their sensing performances. The effective detection of high explosive RDX with extremely low vapor pressure is achieved by an indirect route *via* fast and highly sensitive sensing of a ketone vapor that inevitably co-exists in the explosive product. The IR spectroscopic and guest sorption studies show that LMOF-121 interacts more strongly with acetone than with cyclic ketones as a result of size compatibility, while LMOF-202 adsorbs other ketones more strongly than LMOF-121. The effects of electron and energy transfer processes on both fluorescence enhancement (by ketones)[45] and quenching (by DNT) have been elucidated for LMOF-202, by comparing to LMOF-121 with similar porosity but different electronic structure. Tuning the porosity and electronic properties specifically towards a detection target can significantly improve sensitivity and selectivity. Such strategy can be very helpful in designing highly efficient sensory materials.

Acknowledgements

The RU and UTD authors would like to thank the Department of Energy, Office of Basic Energy Sciences, Materials Sciences and Engineering Division for its generous support through grant no. DE-FG02-08ER-46491. ZH would also like to thank Prof. Karsten Krogh-Jespersen for the helpful discussion on DFT calculations, Prof. Xinlong Wang for graphic design of Fig. 1, Aaminah b'Hat and David J. Golembieski for reproducing LMOF samples used in this study, and Qihan Gong for help with the adsorption experiments.

Notes and references

1 S. J. Toal and W. C. Trogler, *J. Mater. Chem.*, 2006, **16**, 2871–2883.
2 S. W. Thomas, G. D. Joly and T. M. Swager, *Chem. Rev.*, 2007, **107**, 1339–1386.
3 M. E. Germain and M. J. Knapp, *Chem. Soc. Rev.*, 2009, **38**, 2543–2555.
4 Y. Salinas, R. Martinez-Manez, M. D. Marcos, F. Sancenon, A. M. Costero, M. Parra and S. Gil, *Chem. Soc. Rev.*, 2012, **41**, 1261–1296.

 This journal is © The Royal Society of Chemistry 2014

5 D. Gopalakrishnan and W. R. Dichtel, *J. Am. Chem. Soc.*, 2013, **135**, 8357–8362.
6 P. Kolla, *Angew. Chem., Int. Ed. Engl.*, 1997, **36**, 800–811.
7 J. C. Sanchez and W. C. Trogler, *J. Mater. Chem.*, 2008, **18**, 3143–3156.
8 M. Uchimiya, L. Gorb, O. Isayev, M. M. Qasim and J. Leszczynski, *Environ. Pollut.*, 2010, **158**, 3048–3053.
9 J. R. Cox, P. Müller and T. M. Swager, *J. Am. Chem. Soc.*, 2011, **133**, 12910–12913.
10 M. A. Ivy, L. T. Gallagher, A. D. Ellington and E. V. Anslyn, *Chem. Sci.*, 2012, **3**, 1773–1779.
11 N. Lorenzo, T. Wan, R. Harper, Y.-L. Hsu, M. Chow, S. Rose and K. Furton, *Anal. Bioanal. Chem.*, 2003, **376**, 1212–1224.
12 H. Lai, A. Leung, M. Magee and J. Almirall, *Anal. Bioanal. Chem.*, 2010, **396**, 2997–3007.
13 A. Lan, K. Li, H. Wu, D. H. Olson, T. J. Emge, W. Ki, M. Hong and J. Li, *Angew. Chem., Int. Ed.*, 2009, **48**, 2334–2338.
14 A. Lan, K. Li, H. Wu, L. Kong, N. Nijem, D. H. Olson, T. J. Emge, Y. J. Chabal, D. C. Langreth, M. Hong and J. Li, *Inorg. Chem.*, 2009, **48**, 7165–7173.
15 S. Pramanik, C. Zheng, X. Zhang, T. J. Emge and J. Li, *J. Am. Chem. Soc.*, 2011, **133**, 4153–4155.
16 C. Janiak, *Dalton Trans.*, 2003, 2781–2804.
17 M. D. Allendorf, C. A. Bauer, R. K. Bhakta and R. J. T. Houk, *Chem. Soc. Rev.*, 2009, **38**, 1330–1352.
18 B. Chen, S. Xiang and G. Qian, *Acc. Chem. Res.*, 2010, **43**, 1115–1124.
19 S.-T. Zheng, J. T. Bu, Y. Li, T. Wu, F. Zuo, P. Feng and X. Bu, *J. Am. Chem. Soc.*, 2010, **132**, 17062–17064.
20 Y. Cui, Y. Yue, G. Qian and B. Chen, *Chem. Rev.*, 2012, **112**, 1126–1162.
21 L. E. Kreno, K. Leong, O. K. Farha, M. Allendorf, R. P. Van Duyne and J. T. Hupp, *Chem. Rev.*, 2012, **112**, 1105–1125.
22 J. W. Uebler, A. L. Pochodylo, R. J. Staples and R. L. LaDuca, *Cryst. Growth Des.*, 2013, **13**, 2220–2232.
23 Z. Hu, B. J. Deibert and J. Li, *Chem. Soc. Rev.*, 2014, **43**, 5815–5840.
24 M. M. Wanderley, C. Wang, C.-D. Wu and W. Lin, *J. Am. Chem. Soc.*, 2012, **134**, 9050–9053.
25 N. B. Shustova, A. F. Cozzolino, S. Reineke, M. Baldo and M. Dincă, *J. Am. Chem. Soc.*, 2013, **135**, 13326–13329.
26 G.-B. Li, H.-C. Fang, Y.-P. Cai, Z.-Y. Zhou, P. K. Thallapally and J. Tian, *Inorg. Chem.*, 2010, **49**, 7241–7243.
27 J. He, M. Zha, J. Cui, M. Zeller, A. D. Hunter, S.-M. Yiu, S.-T. Lee and Z. Xu, *J. Am. Chem. Soc.*, 2013, **135**, 7807–7810.
28 H.-L. Jiang, D. Feng, K. Wang, Z.-Y. Gu, Z. Wei, Y.-P. Chen and H.-C. Zhou, *J. Am. Chem. Soc.*, 2013, **135**, 13934–13938.
29 H. Xu, F. Liu, Y. Cui, B. Chen and G. Qian, *Chem. Commun.*, 2011, **47**, 3153–3155.
30 B. Gole, A. K. Bar and P. S. Mukherjee, *Chem. Commun.*, 2011, **47**, 12137–12139.
31 A. K. Chaudhari, S. S. Nagarkar, B. Joarder and S. K. Ghosh, *Cryst. Growth Des.*, 2013, **13**, 3716–3721.
32 J.-D. Xiao, L.-G. Qiu, F. Ke, Y.-P. Yuan, G.-S. Xu, Y.-M. Wang and X. Jiang, *J. Mater. Chem. A*, 2013, **1**, 8745–8752.
33 S. S. Nagarkar, B. Joarder, A. K. Chaudhari, S. Mukherjee and S. K. Ghosh, *Angew. Chem., Int. Ed.*, 2013, **52**, 2881–2885.
34 Y.-S. Xue, Y. He, L. Zhou, F.-J. Chen, Y. Xu, H.-B. Du, X.-Z. You and B. Chen, *J. Mater. Chem. A*, 2013, **1**, 4525–4530.
35 Z. Hu, S. Pramanik, K. Tan, C. Zheng, W. Liu, X. Zhang, Y. J. Chabal and J. Li, *Cryst. Growth Des.*, 2013, **13**, 4204–4207.
36 D. Banerjee, Z. Hu, S. Pramanik, X. Zhang, H. Wang and J. Li, *CrystEngComm*, 2013, **15**, 9745–9750.
37 S. Pramanik, Z. Hu, X. Zhang, C. Zheng, S. Kelly and J. Li, *Chem.–Eur. J.*, 2013, **19**, 15964–15971.
38 D. Banerjee, Z. Hu and J. Li, *Dalton Trans.*, 2014, 10668–10685.
39 Crystal data for $[Zn_2(ofdc)_2(bpy)]\cdot 2.5DMF\cdot 1.25H_2O$ (LMOF-201), $C_{47.5}H_{40}N_{4.5}O_{13.75}Zn_2$, f.w. = 1024.58, monoclinic, space group $P2(1)/c$, a = 13.8166(7) Å, b = 21.7847(12) Å, c = 20.1414(11) Å, β = 103.312(1)°, V = 5899.5(5) Å^3, Solvent accessible volume 52.6%, Z = 4, ρ_{calcd} = 1.154 g cm^{-3}, $F(000)$ = 2106, μ = 0.870 mm^{-1}, monochromatized Mo Kα radiation (λ = 0.71073 Å), T = 100(2) K, $2\theta_{max}$ = 56.42°, reflections collected 59805 (14630 unique, $R_{int.}$ = 0.0760), $R1$ = 0.0822, w$R2$ = 0.2006, GoF = 1.017.†
40 Crystal data for $[Zn_2(hfdc)_2(bpy)]\cdot x$DMA (LMOF-202), $C_{40}H_{24}N_2O_8Zn_2$, f.w. = 791.39, monoclinic, space group $C2/c$, a = 33.559(7) Å, b = 22.171(4) Å, c = 19.706(4) Å, β = 124.022(3)°, V = 12152(4) Å^3, Solvent accessible volume 56.1%, Z = 8, ρ_{calcd} = 0.865 g cm^{-3}, $F(000)$ = 3216, μ = 0.823 mm^{-1}, monochromatized Mo Kα radiation (λ = 0.71073 Å), T = 295(2) K, $2\theta_{max}$ = 50.06°, reflections collected 47666 (10719 unique, $R_{int.}$ = 0.0502), $R1$ = 0.0693, w$R2$ = 0.2322, GoF = 1.048.†
41 M. J. Frisch, *et al.*, *Gaussian 09, Revision C.01*, Gaussian, Inc., Wallingford, CT, 2010. See the ESI† for details and full references.
42 D. Gao, Z. Wang, B. Liu, L. Ni, M. Wu and Z. Zhang, *Anal. Chem.*, 2008, **80**, 8545–8553.
43 S. Ramachandra, Z. D. Popovic′, K. C. Schuermann, F. Cucinotta, G. Calzaferri and L. De Cola, *Small*, 2011, **7**, 1488–1494.
44 A. Saxena, M. Fujiki, R. Rai and G. Kwak, *Chem. Mater.*, 2005, **17**, 2181–2185.
45 Further study on the enhancement mechanism is intended, such as the uptake of each ketone by LMOFs, the possibility of hydrogen atom abstraction from the hfdc ligand under the same condition as the sensing experiments are performed.